

CHEMICAL KINETICS
AND CATALYSIS

Framework-Substituted Sn-MOR Zeolite Prepared
by Multiple pH-Adjusting Co-Hydrolysis As Efficient Catalyst
for *tert*-Butylation of Toluene¹

Fuling Cheng^a, Zhiwei Zhou^{a,*}, Juan Qin^b, Dong Li^a, Jianzong Wang^a, and Wenliang Wu^{a,**}

^aCollege of Chemical Engineering, Nanjing Tech University, Nanjing, 210009 P. R. China

^bTechnology and Finance Service Center of Jiangsu Province, Productivity Center of Jiangsu Province,
Nanjing, 210042 P. R. China

*e-mail: zhiweizhou@njtech.edu.cn

**e-mail: wwl@njtech.edu.cn

Received December 12, 2017

Abstract—A series of Sn-MOR samples with different tin species loadings were prepared via a multiple pH-adjusting co-hydrolysis method. Their properties were characterized by XRD, XRF, UV–Vis, FT-IR, Py-IR, N₂ sorption and SEM techniques. The catalytic performance was evaluated in liquid-phase toluene alkylation with *tert*-butyl alcohol. The characterization results shows that compared to framework destruction of mordenite for the Sn/MOR sample with floccule prepared by ion exchange method, higher relative crystallinity and larger surface area and pore volume for Sn-MOR samples with walnut morphology can be obtained. The doping with tin species can increase the Lewis acidity and decrease the pore size resulting in both higher toluene conversion and *p-tert*-butyltoluene (PTBT) selectivity. The Sn-MOR(0.010) sample shows the highest catalytic performance with toluene conversion of 48.0% and PTBT selectivity of 85.6%. It shows high stability: toluene conversion of 45.3% and PTBT selectivity of 87.2% can be obtained even after 5 consecutive runs.

Keywords: Sn-MOR, multiple adjusting, co-hydrolysis, toluene, *p-tert*-butyltoluene

DOI: 10.1134/S0036024418130095

INTRODUCTION

p-tert-Butyltoluene (PTBT), one of three isomers of *tert*-butyltoluene, is an important chemical intermediates. It can be oxidized to *p-tert*-butylbenzaldehyde and *p-tert*-butylbenzoic acid, which are used in production of fragrances, resins, polyesters or pharmaceuticals. Up to now, PTBT is often prepared by Friedel-Crafts alkylation of toluene with various reagents including isobutylene, *tert*-butyl chloride and *tert*-butyl alcohol using liquid acid catalysts, such as BF₃, AlCl₃, H₂SO₄, HF, or H₃PO₄, etc. [1], which would suffer from some drawbacks regarding both difficult catalyst recovery resulting in environment pollution and severe equipment corrosion. In order to avoid these problems, many solid acid catalysts, such as zeolites, heteroatom mesoporous materials and heteropolyacid supported catalysts have been explored.

In the liquid-phase alkylation of toluene with *tert*-butyl alcohol, zeolites-based materials with high hydrothermal stability and shape selectivity would be promising catalysts because water is formed by intra-

molecular dehydration of *tert*-butyl alcohol [2–8]. The PTBT selectivity over mordenite is higher than over other zeolites owing to the close dimensions of zeolite pores and molecular diameter of PTBT (0.58 nm) [9]. However, its catalytic activity is rather limited because of the low acidity, especially Lewis acidity, which has been proved to be beneficial to the toluene conversion. Therefore, the mordenite based catalysts modified for increasing their Lewis acidity would show good catalytic performance in liquid-phase toluene alkylation with *tert*-butyl alcohol.

Among the modification methods, the introduction of the active components with high Lewis acidity into the framework with good catalytic stability would be a promising strategy, and some heteroatom mordenite catalysts have been prepared by replacing tetrahedrally coordinated sites of parent Si or Al atom under controlled conditions [10–16]. For example, Sn-beta zeolite prepared by incorporation of tetravalent tin into the framework has been proved to be a solid Lewis acid catalyst with high activity in the glucose epimerization, Bayer–Villiger oxidation and glycerol acetalization [17–20]. In addition, since the atomic diameter of tin is larger than that of Si or Al, its

¹ The article is published in the original.

successful incorporation would effectively reduce the pore size of mordenite, which would probably be favorable for the PTBT selectivity [21]. However, the heteroatom Sn-MOR zeolite in situ synthesis has not been widely reported so far, which may be owing to the layered structure of mordenite itself and to the longer Si–O–Sn bonds or higher bond angles strain resulting in the structural distortion [22].

The synthesis of heteroatomic zeolites is affected by a variety of factors, such as synthesis routes, reaction conditions, and the nature of heteroatoms [23]. It is well known that basic conditions (pH 9–13) are essential for the preparation of heteroatom zeolite by the conventional procedure, when the metal oxide is usually formed resulting in the difficulty of incorporation into the zeolite framework for the metal atom. On the contrary, the hydrolysis rate of silica source would be slower under acidic conditions, which can provide more chance to isolate and disperse the metal ion and would be beneficial to the formation of the bond between metal ion and silanol groups followed by crystallization under the basic condition. Thus, the Sn-doped zeolite can be successfully obtained using the above multiple pH-adjusting co-hydrolysis method [22]. The template type would affect severely the structure of the final product. Ionic liquids (ILs) with weak structural orientation ability exhibit an extended hydrogen bond network in the liquid state and a continuous three dimensional network of ionic channels, which can coexist with nonpolar domains created by the grouping of lipophilic alkyl chains. When pH value of sol is less than 7 [24–28], IL can be an effective template for the preparation of mordenite. Therefore, the successful preparation of Sn-MOR zeolite would be possible using ILs as template in a multiple pH-adjusting co-hydrolysis method, which was not reported so far.

In this work, a series of Sn-MOR zeolites were prepared using a multiple pH-adjusting co-hydrolysis method, and their physical chemical properties were characterized by different techniques. Furthermore, their catalytic performance was also investigated in the liquid-phase alkylation of toluene with *tert*-butyl alcohol.

EXPERIMENTAL

Preparation of Catalysts

The Sn-MOR zeolites with different tin species loadings were synthesized by a multiple pH-adjusting co-hydrolysis method described in [24]. In a typical procedure, 8.0 g silicic acid was dissolved in 12.0 g water, and a certain amount of hydrochloric acid (98 wt %) was slowly added with vigorous stirring until pH 0.8–1.0, followed by addition of a preset amount of tin chloride at 298 K for another 24 h. After that, 0.3 g of NaAlO₂ and 4.4 g of 1-butyl-3-methylimidazolium bromide ([BMIm]Br) were simultaneously

added resulting in mixture pH of 5.0–6.0 with continuously stirring for 12 h. Finally, the aqueous NaOH solution (50 wt %) was dropwise added for adjusting the pH of the slurry to 11.9. The resulting gels were transferred into a sealed Teflon-lined autoclave and heated under static conditions at 413 K for 5 days. The final solid product was filtered, dried at 383 K for 24 h, and then calcined at 823 K for 5 h in air stream. The obtained samples are designated as Sn-MOR(*n*), where *n* stands for the molar ratio of tin species to silicon species. For comparison, the MOR zeolite was synthesized in the absence of tin chloride under the above preparation conditions, and the Sn/MOR zeolite was also prepared by ion exchange method with 0.1 mol/L aqueous tin chloride solution (1 g : 10 mL).

Characterizations of Catalysts

The crystalline structures of the prepared samples were characterized by X-ray diffraction analysis (XRD) using a SmartLab diffractometer from Rigaku equipped with a 9 kW rotating anode Cu source at 40 kV and 40 mA with a scan rate of 0.2 deg s⁻¹ in the 2θ range from 5° to 50°. Nitrogen sorption was measured at 77 K using a BEL SORP-MAX instrument. The surface area was calculated by BET method, and the average pore size was determined by BJH method. The chemical compositions of samples were obtained using ADVANT'XP X-ray fluorescence (XRF) spectrometer (ZSX Primus II). FT-IR spectra were recorded on a Nicolet 360 instrument. The sample was pretreated in 10⁻² Pa vacuum at 573 K for 3 h and then cooled down to room temperature for adsorbing pyridine for 2 h. After that, the temperature was raised to 473 K for 1 h to remove the physisorbed pyridine, and the Py-IR spectra were measured at room temperature. Diffuse reflectance UV–Vis spectra were measured on PE Lambda 950 UV–Vis spectrophotometer. The wavelength range was from 200 to 800 nm and BaSO₄ was used as a reference compound. Particle morphology of the samples was observed by SEM using a Hitachi S-4800 field-emission scanning electron microscope (FESEM).

Catalytic Tests

The catalytic alkylation of toluene with *tert*-butyl alcohol was carried out in a 0.1 L stainless steel autoclave with a magnetically driven impeller. The catalyst sample (0.2 g) was added into a mixture of 9.35 g of *n*-hexane with 2.0 g toluene and 3.22 g *tert*-butyl alcohol. The above mixture was sealed in the reactor and flushed for multiple times with nitrogen to replace air. Then the mixture was heated to the preset reaction temperature of 453 K with the initial pressure of 1.0 MPa. After 5 h, the mixture was cooled down to room temperature, and the catalyst was removed by filtration. The reaction mixture was analyzed on a SP-6890 gas chromatograph equipped with a SE-30

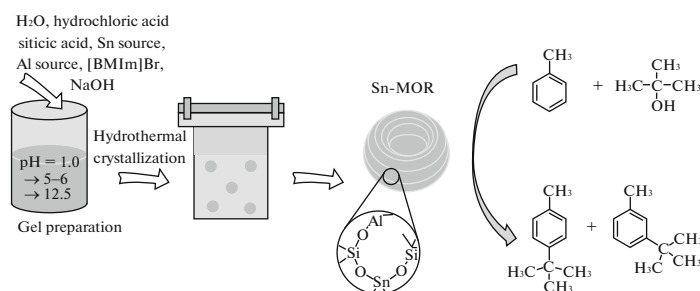


Fig. 1. Schematic diagram of the synthesis procedure of framework-substituted Sn-MOR zeolite for toluene alkylation with *tert*-butyl alcohol.

column (0.25 $\mu\text{m} \times 50$ m) and a flame ionization detector (FID). To estimate the catalyst stability, the catalyst after previous run was collected by filtration and reused without any further treatment. Schematic diagram of the synthesis procedure of framework-substituted Sn-MOR zeolite is shown in Fig. 1.

RESULTS AND DISCUSSION

Catalyst Characterization

XRD patterns for different Sn-MOR samples are shown in Fig. 2. The Sn-MOR(0) sample shows the identical characteristic peaks with the simulated samples, suggesting the successful preparation of mordenite [24, 29]. Although the intensity of these peaks was slightly decreased with the tin species loading increasing [30], the characteristic peaks can be clearly observed for all the Sn-MOR samples, which indicated that the incorporation of tin species would not severely affect the framework. However, when the molar ratio of Sn/Si reaches 0.020, some other peaks corresponding to other impurities appeared, which may be probably unfavorable to its catalytic performance. In addition, no obvious peaks corresponding to tin species can be observed owing to either their highly dispersion or small particles size undetected by XRD patterns. However, the intensities of these characteristic peaks for Sn/MOR(0.010) sample prepared by ion exchange were very low, suggesting its breakdown of the mordenite framework, suggesting that the ion exchange process destroys the structure and crystallinity of MOR. In addition, the weak characteristic peaks centered at $2\theta = 26.6^\circ$, 33.9° , and 37.9° appeared, indicating that the SnO_2 particles would be formed by ion exchange method.

Table 1 was the textural parameters for different samples. For the pure Sn-MOR(0) sample, the surface area of $441.5 \text{ m}^2 \text{ g}^{-1}$, pore volume of $0.23 \text{ cm}^3 \text{ g}^{-1}$ and average pore size of 0.76 nm can be obtained. The molar ratio of SiO_2 to Al_2O_3 would be promoted by the incorporation of tin species suggesting that the aluminum into the framework of pure MOR zeolite would be substituted by the tin species resulting in the smaller pore volume and average pore size, which is owing to

the bigger atom radius of tin than that of aluminum. The surface area would slightly increase with increasing tin species load, further indicating that the tin species incorporated into the framework. For Sn/MOR(0.010) sample, the surface area is only $253.1 \text{ m}^2 \text{ g}^{-1}$, which can be attributed to the destruction of the framework resulting in the average pore size of 0.81 nm and pore volume of $0.11 \text{ cm}^3 \text{ g}^{-1}$. At the same time, the molar ratio of SiO_2 to Al_2O_3 for Sn/MOR(0.010) sample slightly increased from 18.1 to 19.0, indicating that the dealumination would happen in the ion exchange method, which may be owing to the weak acidity of aqueous tin chloride solution resulting in partial formation of substitution of aluminum species by tin species.

Figure 3 shows the UV-Vis DRS spectra for different Sn-MOR samples. For the Sn-MOR(0) sample, no obvious absorption band in the region of 200–800 nm can be observed. However, a new absorption band centered at about 210 nm corresponding to the tetrahedrally coordinated tin species for Sn-

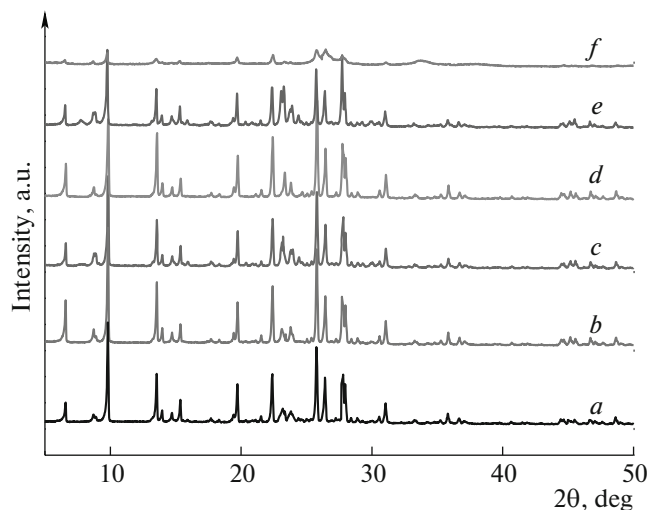


Fig. 2. XRD patterns for different Sn-MOR samples; (a) Sn-MOR(0); (b) Sn-MOR(0.0025); (c) Sn-MOR(0.005); (d) Sn-MOR(0.010); (e) Sn-MOR(0.020); (f) Sn/MOR(0.010).

Table 1. Textural parameters for different Sn-MOR samples

Samples	S_{BET} ($\text{m}^2 \text{g}^{-1}$) ^a	V ($\text{cm}^3 \text{g}^{-1}$) ^b	D (nm) ^c	Sn/Si(molar ratio) ^d	$\text{SiO}_2/\text{Al}_2\text{O}_3$ (molar ratio) ^d
Sn-MOR(0)	441.5	0.23	0.76	0	18.1
Sn-MOR(0.0025)	476.3	0.23	0.71	0.0022	18.7
Sn-MOR(0.005)	478.0	0.22	0.69	0.0042	19.1
Sn-MOR(0.010)	482.9	0.21	0.63	0.0055	20.5
Sn-MOR(0.020)	497.1	0.19	0.52	0.0070	24.2
Sn/MOR(0.010)	253.1	0.11	0.81	0.0053	19.0

^aBET surface areas, ^b $P/P_0 = 0.99$, ^caverage pore size, ^dXRF.

MOR(0.0025) sample emerged. No obvious absorption band centered at 250 nm corresponding to tin dioxide can be observed, suggesting its total incorporation [31–33]. With increasing tin species loading, the band intensity became stronger, indicating that more tin species were successfully tetrahedrally incorporated, but some new absorption band centered between 230 and 300 nm emerged, suggesting some hexahedrally coordinated tin species or tin dioxide were formed, which were either highly dispersed or too small to be detected by XRD resulting in the decreasing relative crystallinity of mordenite. At the same time, it was found that no obvious bands centered at 300–450 nm corresponding to the bulky SnO_2 particles even for Sn-MOR(0.020) sample were present. Compared to the Sn-MOR(0.010) sample, the weaker absorption band centered at about 210 nm for the Sn/MOR(0.010) sample can also appear even though the tin species were the same, which is owing to the dealumination by aqueous tin chloride resulted in the partial substitution of aluminum hole by tin species. However, a broad band centered at 300–450 nm can also be observed, suggesting that some bulky SnO_2

particles were formed [34], which is consistent with the XRD results. Therefore, the difference for the tin species between the two samples with the same content would strongly affect the catalytic performance in the *tert*-butylation of toluene.

FT-IR spectra for different Sn-MOR samples are shown in Fig. 4. Compared to the Sn-MOR(0) sample, a weak absorption band centered about at 960 cm^{-1} for Sn-MOR(0.0025) sample corresponding to the Si–O–Sn vibrations [35–37] based on the results of UV–Vis DRS spectra was observed, although it can be assigned to the Si–OH [38]. In addition, the peak would become weaker and gradually disappear with increasing tin species loading, which is consistent with literature [39]. At the same time, the bands centered 461 , 814 , and 1102 cm^{-1} for Sn-MOR(0) sample, which is owing to the Si–O–Si bending mode, symmetric stretching vibration of Si–O–Si and Si–O–Si vibrational stretching [40], respectively, would be somewhat red-shifted to lower wavenumber because of the larger atomic weight of Sn and the longer Sn–O band [22], which further indicated that the interaction between tin and silicon [41] resulting in the successful incorporation of tin species into the framework of mordenite.

Figure 5 shows Py-IR spectra of different Sn-MOR samples after pyridine adsorption. The bands at 1445 and 1545 cm^{-1} are attributed to the interactions between Lewis and Brønsted acid sites and pyridine, respectively [42–44]. It can be seen from Fig. 5 that the pure mordenite Sn-MOR(0) sample has mainly Lewis acidity. However, the Lewis acidity increased remarkably after incorporation of tin species, which increases with increasing tin species load resulting in promoting catalytic performance. For Sn/MOR(0.010) sample, the Lewis acidity slightly increased, which may be owing to the substitution of aluminium species by tin species with stronger acidity.

The morphology of these samples was studied by SEM, and the results are shown in Fig. 6. A plate morphology with rectangle for Sn-MOR(0) sample was observed. After incorporation of tin species into the framework of mordenite, the morphology gradually changed into spherical, and more and more spherical

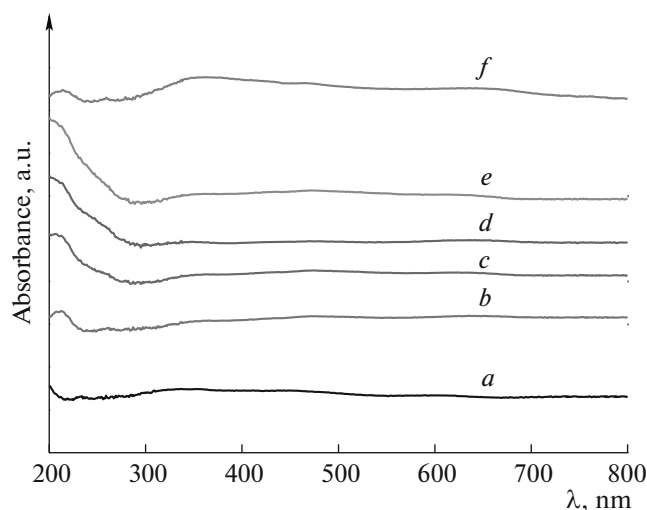


Fig. 3. UV–Vis DRS spectra for different Sn-MOR samples; (a–f) see Fig. 2.

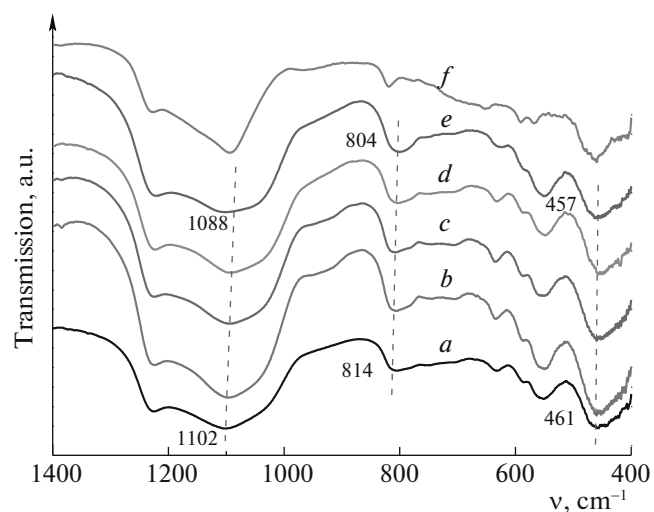


Fig. 4. FT-IR spectra for different Sn-MOR samples; (a–f) see Fig. 2.

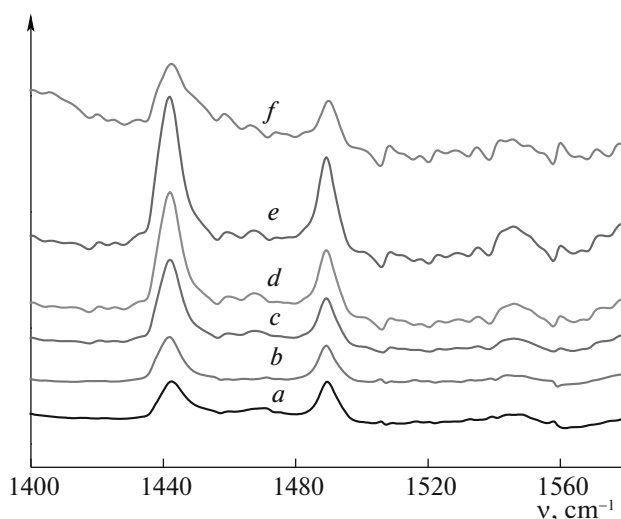


Fig. 5. FT-IR spectra of pyridine-adsorbed for different Sn-MOR samples; (a–f) see Fig. 2.

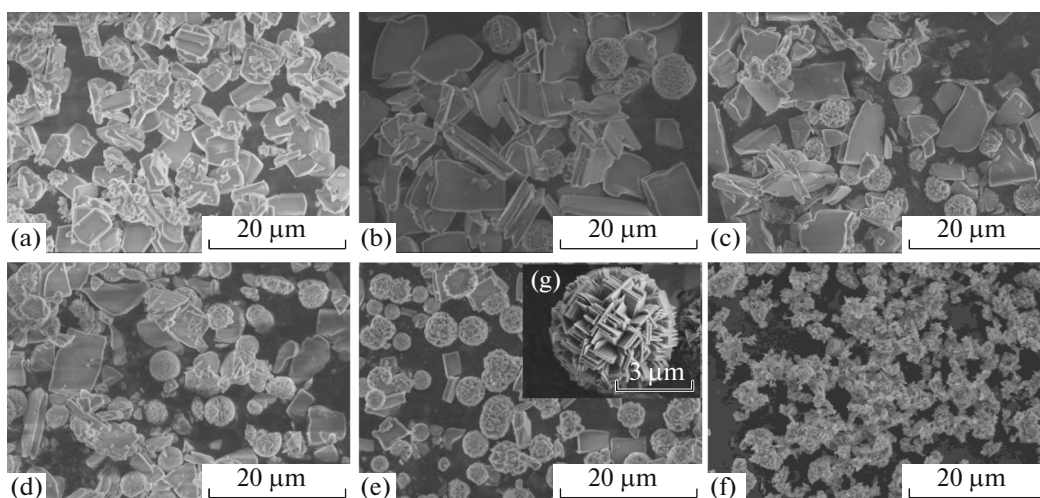


Fig. 6. SEM images for different Sn-MOR samples; (a–f) see Fig. 2.

particles with a diameter of $\sim 5 \mu\text{m}$ would be observed with the tin species loading increase. Figure 6g shows the high resolution image for Sn-MOR(0.020) sample. The walnut morphology was a result of the aggregation with small-sized flake-like crystal, which may be owing to the acceleration the nucleation and growth by the introduction of tin species into the Al-rich system resulting in its specific surface areas increase [45]. The floccule can be obtained for Sn/MOR(0.010) sample shown in Fig. 6f owing to the partial collapse of mordenite framework by the ion exchange method.

Catalytic Performance

The catalytic performances of different samples in the alkylation of toluene with *tert*-butyl alcohol are listed in Table 2. In all cases, the main products are

identified as PTBT and *meta-tert*-butyltoluene (MTBT). However, *ortho-tert*-butyltoluene (OTBT) cannot be found in the products, which is attributed to the steric hindrance between methyl and voluminous *tert*-butyl group. DTBT is 3,5-di-*tert*-butyltoluene, whose *tert*-butyl groups are both in the *meta* positions. It can be seen from Table 2 that toluene conversion of 19.3% and PTBT selectivity of 71.9% for Sn-MOR(0) sample can be obtained. With increasing tin species loading, the conversion of toluene increased, and then decreased at higher tin loadings. The Sn-MOR(0.010) sample gives a toluene conversion of 48.0%, which is 2.5 times than that over pure Sn-MOR(0) sample and much higher than with other samples owing to its appropriate surface area, pore volume and Lewis acidity. Toluene conversion of 34.3% was obtained for the Sn-MOR(0.020) sample with highest acid amount,

Table 2. Catalytic performances of different samples in the alkylation of toluene with *tert*-butyl alcohol

Catalysts	Toluene conversion, %	Distribution of products, mol %				S_{PTBT} , %*
		OTBT	MTBT	PTBT	DTBT	
Sn-MOR(0)	19.3	—	27.1	69.5	3.4	71.9
Sn-MOR(0.0025)	27.1	—	23.8	74.4	1.8	75.8
Sn-MOR(0.005)	39.5	—	18.4	78.6	3.0	81.0
Sn-MOR(0.010)	48.0	—	14.0	83.2	2.8	85.6
Sn-MOR(0.020)	34.3	—	22.5	71.3	6.2	76.0
Sn/MOR(0.010)	8.9	—	39.6	56.3	4.1	58.7

Reaction conditions: $w(\text{toluene})/w(\text{catalyst}) = 10$; calcination temperature of catalyst 823 K; $n(\text{toluene}) : n(\text{tert-butyl alcohol}) : n(n\text{-hexane}) = 1 : 2 : 5$; reaction temperature 453 K; initial pressure 1.0 MPa; reaction time 5 h.

* S_{PTBT} : the molar ratio of PTBT to mono-TBT.

which may be owing to the smaller pore size (0.52 nm) than PTBT molecular diameter (0.58 nm) resulting in the reaction only on the outer surface. The selectivity to PTBT increases with increasing tin species loading. Selectivity value of 85.6% can be obtained for the Sn-MOR(0.010) sample, and it would be dropped with the tin species further increasing. However, a toluene conversion of only 8.9% and PTBT selectivity of 58.7% for Sn/MOR(0.010) sample were observed because of the destruction of framework by ion exchange of tin species although the tin species are almost the same as for the Sn-MOR(0.010) sample.

Figure 7 shows the catalytic stability of Sn-MOR(0.010) catalyst in the alkylation of toluene with *tert*-butyl alcohol. It can be seen from Fig. 7 that toluene conversion decreased slightly and it can also reach up to 45.3% even after 5 consecutive runs. On the contrary, PTBT selectivity would be slightly promoted owing to the blocking of the pores probably of coke formed by oligomerization of isobutene followed by

carbonization. The above results indicated that the Sn-MOR(0.010) catalyst shows high catalytic stability, which would provide a good application prospect in the industrial process.

CONCLUSION

In this paper, Sn-doped mordenite with different tin species loadings were successfully via a multiple pH-adjusting co-hydrolysis method. Tin species can be incorporated into tetrahedral positions of the mordenite framework by substitution of aluminum resulting in promoting its Lewis acidity. Compared to Sn/MOR sample with floccule morphology prepared by ion exchange method, the Sn-MOR samples with walnut morphology can be obtained. The catalytic performances in the toluene alkylation with *tert*-butyl alcohol for Sn-MOR catalysts are much higher than that of pure mordenite. The catalyst activity remains high even after 5 consecutive runs. The described method can be valuable for industrial applications requiring solid acid catalysts.

ACKNOWLEDGMENTS

This work was supported by Jiangsu Planned Projects for Postdoctoral Research Funds (1302121C); Open Project of Beijing Key Laboratory for Enze Biomass and Fine Chemicals; Project Funded by the Priority Academic Program Development of Jiangsu Higher Education Institutions.

REFERENCES

1. S. Ostrowski and J. C. Dobrowolski, *J. Mol. Catal., A* **293**, 86 (2008).
2. W. Alabi, L. Atanda, R. Jermy, and S. Al-Khattaf, *Chem. Eng. J.* **195**, 276 (2012).
3. S. Al-Khattaf, S. Rabiou, N. M. Tukur, and R. Alnaizy, *Chem. Eng. J.* **139**, 622 (2008).
4. C. S. Cundy and P. A. Cox, *Chem. Rev.* **34**, 663 (2003).

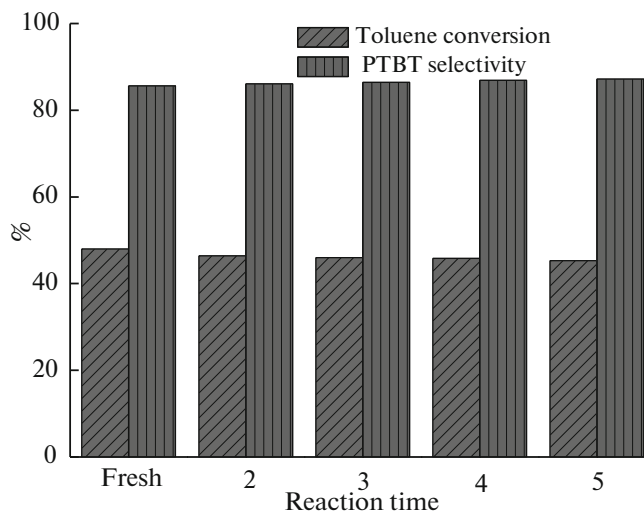


Fig. 7. Catalytic stability for Sn-MOR(0.010) catalyst in the alkylation of toluene with *tert*-butyl alcohol.

5. K. Liu, S. Xie, G. Xu, Y. Li, S. Liu, and L. Xu, *Appl. Catal.*, A **383**, 102 (2010).
6. Y. Liu, L. Xu, B. Xu, Z. Li, L. Jia, and W. Guo, *J. Mol. Catal.*, A **297**, 86 (2009).
7. A. Llanos, L. Melo, F. Avendaño, A. Montes, and J. L. Brito, *Catal. Today* **133**, 20 (2008).
8. B. Xue, Y. Li, and L. Deng, *Catal. Commun.* **10**, 1609 (2010).
9. C. Wang, L. Fan, Y. Shen, D. Liu, and S. Xu, *Chem. React. Eng. Tech.* **28**, 50 (2012).
10. U. Mogera, M. Gedda, S. J. George, and G. U. Kulkarni, *ACS Appl. Mater. Inter.* **9**, 37 (2017).
11. Y. Yang, J. Ding, C. Xu, W. Zhu, and P. Wu, *J. Catal.* **325**, 101 (2015).
12. E. Finocchio, T. Montanari, C. Resini, and G. Busca, *J. Mol. Catal.*, A **204**, 535 (2003).
13. T. Q. Silva, M. B. D. Santos, A. A. C. Santiago, D. O. Santana, F. T. Cruz, H. M. C. Andrade, and A. J. S. Mascarenhas, *Catal. Today* **289**, 38 (2017).
14. D. Pietrogiamomi, M. C. Campa, and M. Occhiuzzi, *Catal. Today* **227**, 116 (2014).
15. K. Sun, W. Su, F. Fan, Z. Feng, T. A. Jansen, R. A. van Santen, and C. Li, *J. Phys. Chem. A* **112**, 1352 (2008).
16. J. Xie, H. Wen, W. Zhang, Y. Zhou, and J. Wang, *CrystEngComm.* **18**, 1164 (2016).
17. A. Corma, L. T. Nemeth, M. Renz, and S. Valencia, *Nature (London, U.K.)* **412**, 423 (2001).
18. E. Janiszewska, S. Kowalak, W. Supronowicz, and F. Roessner, *Mesoporous Mater.* **117**, 423 (2009).
19. U. R. Pillai and E. Sahle-Demessie *J. Mol. Catal.*, A **191**, 93 (2003).
20. P. Wolf, M. Valla, A. J. Rossini, A. Comas-Vives, F. Núñez-Zarur, B. Malaman, A. Lesage, L. Emsley, C. Coperet, and I. Hermans, *Angew. Chem., Int. Ed.* **53**, 10179 (2014).
21. P. Fejes, J. B. Nagy, K. Kovács, and G. Vankó, *Appl. Catal.*, A **145**, 155 (1996).
22. J. Gu, Y. Wu, Y. Jin, and J. Wang, *J. Porous Mater.* **20**, 7 (2013).
23. W. Fan, R. G. Duan, T. Yokoi, P. Wu, Y. Kubota, and T. Tatsumi, *J. Am. Chem. Soc.* **130**, 10150 (2008).
24. Z. Ma, J. Xie, J. Zhang, W. Zhang, Y. Zhou, and J. Wang, *Microporous Mesoporous Mater.* **224**, 17 (2016).
25. M. G. D. Pópolo, C. L. Mullan, J. D. Holbrey, C. Hardacre, and P. Ballone, *J. Am. Chem. Soc.* **130**, 7032 (2008).
26. T. Gutel, C. C. Santini, A. A. Pádua, B. Fenet, Y. Chauvin, J. N. Canongia Lopes, F. Bayard, M. F. Costa Gomes, and A. Pensado, *J. Phys. Chem. B* **113**, 170 (2008).
27. A. A. Pádua, M. F. Costa Gomes, and J. N. Canongia Lopes, *Accounts. Chem. Res.* **40**, 1087 (2007).
28. P. S. Campbell, C. C. Santini, D. Bouchu, B. Fenet, K. Philippot, B. Chaudret, A. A. Padua, and Y. Chauvin, *Phys. Chem. Chem. Phys.* **12**, 4217 (2010).
29. N. Khandan, M. Kazemeini, and M. Aghaziarati, *Catal. Lett.* **129**, 111 (2009).
30. D. Karthikeyan, R. Atchudan, and R. Sivakumar, *Chem. Chin. J. Catal.* **37**, 1907 (2016).
31. J. Dijkmans, M. Dusselier, W. Janssens, M. Trekels, A. Vantomme, E. Breynaert, C. Kirschhock, and F. Bert Sels, *ACS Catal.* **6**, 31 (2016).
32. Z. Zhou, P. Yu, J. Qin, W. Wu, L. Xu, Z. Gu, and X. Liu, *J. Porous Mater.* **23**, 239 (2015).
33. Z. Zhou, Y. Yu, P. Yu, J. Qin, S. Dai, and W. Wu, *React. Kinet. Mech. C* **120**, 295 (2016).
34. M. Khaled, A. Chutia, J. Callison, P. P. Wells, E. K. Gibson, A. M. Beale, C. R. A. Catlow, and R. Raja, *J. Mater.*, A **4**, 5706 (2016).
35. E. G. Vaschetto, G. A. Pecchi, S. G. Casuscelli, and G. A. Eimer, *Microporous Mesoporous Mater.* **265**, 219 (2016).
36. M. Rasouli, H. Atashi, D. Mohebbi-Kalhari, and N. Yaghobi, *Taiwan Inst. Chem. E* **78**, 438 (2017).
37. M. Khatamian, A. Yavari, A. Akbarzadeh, and E. Alizadeh, *Mater. Sci. Eng., C* **21**, 1212 (2017).
38. T. D. Courtney, C. C. Chang, R. J. Gorte, R. F. Lobo, W. Fan, and V. Nikolakis, *Microporous Mesoporous Mater.* **210**, 69 (2015).
39. P. Fejes, J. B. Nagy, K. Kovács, and G. Vankó, *Appl. Catal. A* **145**, 155 (1996).
40. B. Li, Z. Xu, F. Jing, S. Luo, and W. Chu, *Appl. Catal. A* **533**, 17 (2017).
41. M. Dong, J. Wang, and Y. Sun, *Microporous Mesoporous Mater.* **43**, 237 (2001).
42. J. Li, P. Miao, Z. Li, T. He, D. Han, J. Wu, Z. Wang, and Z. Wu, *Energ. Convers. Manage.* **93**, 259 (2015).
43. S. A. Al-Bogami and H. I. de Lasa, *Fuel* **108**, 490 (2013).
44. X. S. Zhao, M. G. Q. Lu, and C. Song, *J. Mol. Catal. A* **191**, 67 (2003).
45. Y. Mao, Y. Zhou, H. Wen, J. Xie, W. Zhang, and J. Wang, *New. J. Chem.* **38**, 3295 (2014).